# Fully-inverted piezoresponse hysteresis loops mediated by charge injection in $0.29Pb(In_{1/2}Nb_{1/2})O_3-0.44Pb(Mg_{1/3}Nb_{2/3})O_3-0.27PbTiO_3$ single crystals

Qian Li,[1] Yun Liu,[1,a)] Jason Schiemer,[1] Paul Smith,[1] Zhenrong Li,[2] Ray L. Withers,[1] and Zhuo Xu[2]
[1]*Research School of Chemistry, The Australian National University, ACT 0200, Australia*
[2]*Electronic Materials Research Laboratory (EMRL), Xian Jiaotong University, Shaanxi 710049, People's Republic of China*

(Received 10 December 2010; accepted 6 February 2011; published online 4 March 2011)

The domain structure and local switching behavior of ternary relaxor (001) $0.29Pb(In_{1/2}Nb_{1/2})O_3-0.44Pb(Mg_{1/3}Nb_{2/3})O_3-0.27PbTiO_3$ single crystals are studied using piezoresponse force microscopy. The as-grown crystals exhibit a labyrinthine domain pattern similar to other relaxor-based ferroelectrics. Abnormally switched domains are observed for both positive and negative tip-voltages, with sign-dependent thresholds and growth rates on the poled crystals. Further piezoresponse hysteresis loop measurements show that fully inverted loops can be observed under high switching voltages, mediated by injected charge fields. The dynamic behavior of the observed abnormal switching is qualitatively analyzed and the underlying mechanisms discussed. © *2011 American Institute of Physics*. [doi:10.1063/1.3562034]

Over recent years, piezoresponse force microscopy (PFM) has become a powerful tool for visualizing as well as manipulating ferroelectric domains on length scales down to the nanoscale.[1] An intriguing aspect of recent PFM studies has been the observation of abnormal domain switching, i.e., domain inversion to the direction against the applied field, typically accompanied by peculiar local piezoresponse (*PR*) hysteresis loops. Abplanalp *et al.*[2] reported this phenomenon in $BaTiO_3$ thin films and attributed it to ferroelastoelectric switching due to the coupling between applied electric field and stress. Later, similar results were reported in several other ferroelectric materials,[3–7] and a more universal model based on charge injection was proposed.[4,5] In this model, the charge carriers enter the sample through the tip-surface junction (via Schottky emission or the tunneling effect) during the application of voltage. These carriers then drift under the electric field and become localized at trap centers within the ferroelectrics thereby forming an anti-parallel internal field. After the tip is grounded, this internal field induces the nucleation and growth of inversely switched domains (ISDs). These studies have elucidated the growth mechanism of ISDs but provided little insight into their dynamic behavior.

In this contribution, we extend PFM studies to ternary relaxor ferroelectric $0.29PbIn_{1/2}Nb_{1/2}O_3-0.44PbMg_{1/3}Nb_{2/3}O_3-0.27PbTiO_3$ (PIMNT) single crystals. The abnormal domain switching behavior of the crystals is investigated and the results discussed with reference to the charge injection model. Several phenomena related to this interpretation are reported and lead to a greater understanding of the interaction between the tip and ferroelectrics in PFM.

The PIMNT single crystals were grown as described elsewhere.[8] (001)-oriented samples were cut and optically polished to a thickness of ~0.6 mm. Silver paint was applied to the (001) surfaces to facilitate external poling (10 kV/cm, 2 min) and then removed by dissolving in acetone. PFM investigations were performed on a commercial atomic force microscope (Cypher, Asylum Research) using Olympus Pt-coated Si probes (spring constant $k \sim 2$ N/m, tip radius ~25 nm). For domain imaging, a 10 kHz ac modulation voltage (amplitude $V_{ac}=1-3$ V) was applied with a contact set point ~150 nN. The MicroAngelo nanolithography procedure (Asylum Research) was used for control of the point-array poling experiments. To acquire local *PR* loops, a 600 kHz ac signal ($V_{ac}=3$ V, phase offset=180°) was superimposed on a 0.5 Hz triangular square-stepping wave with bias window up to ±100 V.[9] Both the writing time and reading time were 25 ms, and each loop was averaged over five consecutive cycles. The polarization hysteresis loop (*P-E*) of the sample was also measured with an aixACCT TF 2000 system.

Figure 1(a) shows the surface morphology of the as-grown crystals. The existence of height contrast implies that upwards and downwards polarized domains polish at different rates. Figures 1(b) and 1(c) show the PFM amplitude and phase, respectively, from the same area. The features observed are close to ideal PFM contrast: amplitudes drop to zero across domain boundaries while phases change by 180°. The as-grown PIMNT crystal exhibits a labyrinthine domain pattern with typical widths of 50–150 nm, which resembles that of $(Pb,La)(Zr,Ti)O_3$ ceramics[10] as well as $Pb(Zn_{1/3}Nb_{2/3})O_3-PbTiO_3$ and $Pb(Mg_{1/3}Nb_{2/3})O_3-PbTiO_3$.[5,11] This confirms the existence of a typical labyrinthine type relaxor ferroelectric domain configuration.

Figure 2(a) shows a phase image of an externally poled PIMNT single crystal. As expected, the crystal exhibits an essentially homogenous, single domain, downwards polarized state after poling. Traces of unswitched spots do remain, presumably due to air gaps around the electrodes. An illustration of the procedure for twelve-point array poling is overlaid on Fig. 2(a). In this procedure, the grounded tip travels

a)Electronic mail: yliu@rsc.anu.edu.au.

 

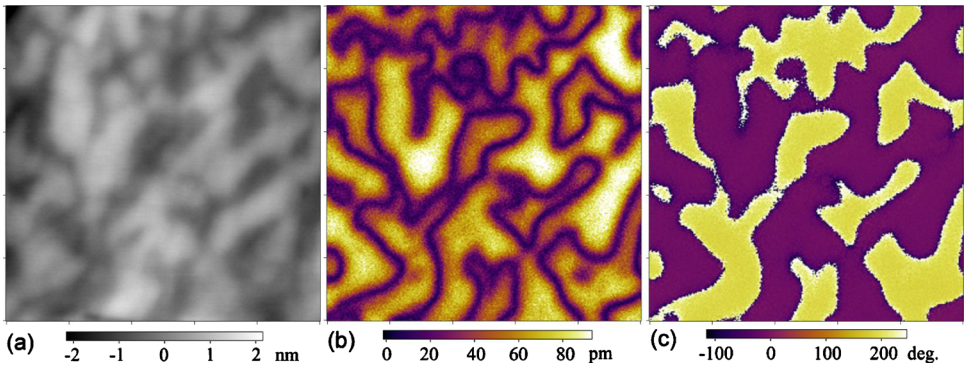


FIG. 1. (Color online) (a) Surface morphology, (b) PFM amplitude and (c) PFM phase images of unpoled (001)-PIMNT single crystals. The image size is $1\times1$ $\mu m^2$.

along the plotted trajectory in contact mode, dwelling on each point for different duration times with an applied dc voltage. A higher set point ~200 nN was used here to ensure good electrical contact while still eliminating possible mechanical stress effects. The phase image taken immediately after poling is shown in Fig. 2(b). Typically, we observe an ISD in the center of the normally switched circular area above a threshold of −15 V. Moreover, the three annuli created under −60 V were cut (poled) along the tip trajectory with the center one cut a second time during tip withdrawal. Further results confirm that this occurs when the poling voltage is ≥−50 V (not shown), suggesting that the injected charge carriers have diffused into a large volume (radius > ~300 nm for −60 V) so that the normally switched domains in the annular boundaries can be inverted again by the internal fields. This tip trajectory-related phenomenon is consistent with the results of Kim *et al.*[6] It provides a useful method to estimate the effective diffusion distance of the injected carriers. If the thickness of the sample was below 300 nm, the injected carriers would sink into the bottom electrode and ISDs would not be observed, under a spherical distribution assumption for the injected charges.

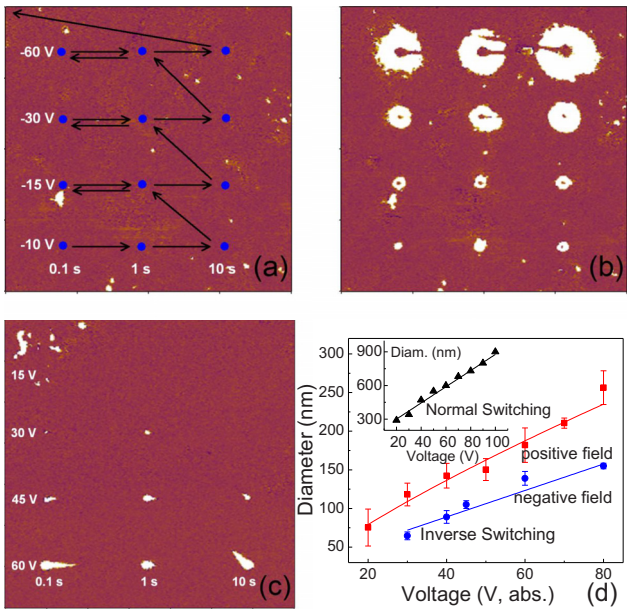


FIG. 2. (Color online) (a) PFM phase images of externally poled PIMNT single crystals ($4\times4$ $\mu m^2$), on which an illustration of the twelve-point poling experiments is overlaid, (b) phase image after positive field poling of the same area, (c) PFM phase image after negative field poling of a different area ($3.5\times3.5$ $\mu m^2$), and (d) diameters of normal (inset) and inverse switching domains as a function of applied voltage.

We also applied positive voltages through the tips to check the feasibility of parallel field poling. As shown in Fig. 2(c), the polarization of the center areas beneath the tip can be inverted after the voltage reaches 30 V, and the features relating to tip trajectory are also visible. This result is quite different to that in a previous report,[5] in which the inverse switching occurs only for negative tip voltages in $Pb(Zn_{1/3}Nb_{2/3})O_3-PbTiO_3$. The field-dependent diameters of the normal domains and ISDs for 1 s pulse durations are plotted in Fig. 2(d). The growth of the normal domains shows a good linear correlation with applied voltage. It has been proposed that PFM tip-created domains generally follow linear voltage-dependent sidewise growth dynamics.[12] Assuming the effective injected charge field increases linearly with applied voltage, we can thus deduce the growth rate of ISDs by linear fitting. Apart from a lower threshold, the ISDs at positive fields ($V<0$) grow ~1.5 times faster than at negative fields ($V>0$), implying that the internal field builds more quickly for the former as voltage increases. In addition, our results show no clear duration dependence of the ISD sizes on voltage, presumably because the injected charges saturate quickly.[7]

To obtain further insight into the dynamic domain switching behavior of poled PIMNT, we also measured *PR* loops at several random locations. These local *PR* loops show consistent results. Figures 3(a)–3(d) show the *PR* loops at a typical location. As can be seen, a well saturated *PR* loop is observed at a low maximum voltage of 10 V, and the loop is distinctly shifted downwards along the *PR* axis resulting in $PR(-) \sim 2PR(+)$. This suggests that the local domain switching is constrained by the original downward polarization state.[13] Considering that the macroscopic *P-E* loop [Fig. 3(e)] is offset along the field axis, common in acceptor-doped bulk ferroelectrics, we infer the presence of point defects inside the crystals probably linked to the growth process. During poling these defect-dipoles align preferentially along the poling direction, and generate a built-in field additionally contributing to the poled state.[14]

For a maximum tip voltage of ±20 V, the *PR* loop becomes irregular with self-crossings close to its maximum.[15] $PR(+)$ and $PR(-)$ decrease after about 12 V and −10 V, respectively, although retaining their signs throughout [Fig. 3(b)]. This implies the onset of increasing internal carrier fields for both polarities. When the maximum voltage is increased to ±30 V, however, the signs of both $PR(+)$ and $PR(-)$ switch [Fig. 3(c)], in agreement with the results of previous poling experiments.

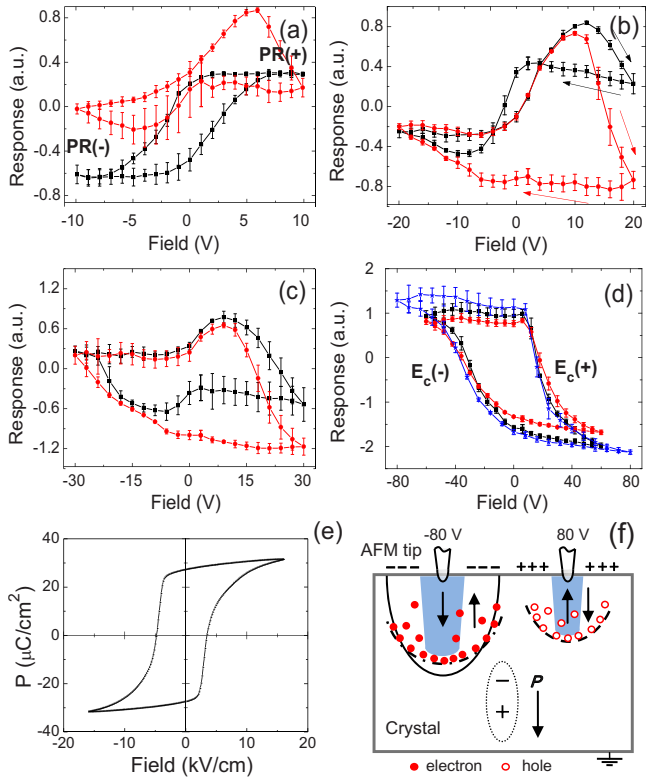


FIG. 3. (Color online) [(a)–(d)] local *PR* loops measured at a single location under increasing (squares) and decreasing (circles) sequences of tip voltages: (a) ±10 V, (b) ±20 V, (c) ±30 V, and (d) ±60 V with an extra loop under ±80 V (star), (e) *P-E* hysteresis loop measured at 1 Hz, and (f) domain configurations after writing voltages of ±80 V (not to scale). The plus and minus signs represent free surface screening charges. The dashed and dashed-dotted lines show the diffusion fronts of injected holes and electrons, respectively. The elliptical dotted line with the plus and minus sign represents polarization charges.

On further increasing the maximum voltage, the *PR* loops become essentially regular again until they eventually saturate at voltages of 60–80 V [Fig. 3(d)]. These *PR* loops are then well defined and opposite to the external fields, verifying that they are mediated by the fields of the injected charges. The apparent coercive fields $E_c(-) \sim -35$ V and $E_c(+) \sim 15$ V [Fig. 2(d)] correspond approximately to the threshold voltages at which ISDs can be observed in the PFM images. Note that the (maximum) *PR* values for both polarities are thereby significantly enhanced. It is therefore, believed that the defect-dipoles mentioned above are fully relaxed under high switching fields, and that cylindrical domains are created by the internal fields, as illustrated schematically in Fig. 3(f). To obtain precise parameters describing domain configurations in these cases, however, requires a quantitative deconvolution of the *PR* hysteresis loops.[16] Note also that the positive half cycles are expanded compared to the negative half cycles, implying better polarization stability in the former case.[17] We infer that for the positive cycles upward polarization can be readily screened by the Pt-coated tip, while the screening of the downward domain with larger size relies more on the migration of surface charges.[18] The inverted domains are under-screened because the free screening surface charges are collected by the grounded tip prior to their switching.[4] Thus different surface screening conditions affect the shapes of the loops.

When sweeping the fields in the reverse sequence, the *PR* loops only match those from the increasing sequence in half cycles, while there are big lags in the other half cycles [Figs. 3(a)–3(c)]. This effect comes from each cycle having remnant injected electrons which cannot be completely compensated when cycling under a lower field, due to shorter diffusion distances.

As stated initially, the formation of internal charge fields depends on two processes: charge injection and the trapping of injected carriers. In this study, ISDs can be observed for both field polarities. Furthermore, the growth of domains mediated by injected electrons and holes must have parallel dynamic parameters in order to form a fully-inverted *PR* loop. We therefore, infer that the Schottky barrier heights for electrons and holes must be very close, i.e., the Fermi level of the Pt-coated tip lies near the middle of the band gap of the PIMNT single crystals.[19] In the interior, there must be sufficient trap centers available for both electrons and holes. Our preliminary electron spin resonance (ESR) results show a strong paramagnetic $O^-$ center (holes self-trapped at $O^{2-}$ ions) in PIMNT single crystals after PFM studies.[20] Although we cannot definitively attribute its formation to the injected charges.[5]

In summary, we have revealed the labyrinthine domain structures of unpoled (001)-PIMNT single crystals and investigated the inverse switching behavior of the poled crystals. The inverse switching occurs for both signs of the tip voltages, controlled by either electron or hole injection. Fully-inverted *PR* hysteresis loops can be observed under high fields, reflecting the growth dynamics of ISDs for both polarities. We intend to confirm that this is a universal phenomenon in PFM studies, and can potentially be employed in interface-controlled ferroelectric nanodevices.

Q.L., Y.L., and R.L.W. acknowledge financial support from the Australian Research Council (ARC) in the form of an ARC Discovery (Grant No. DP0877069).

[1]*Electrical and Electromechanical Phenomena at the Nanoscale*, edited by S. V. Kalinin and A. Gruverman (Springer, New York, 2007).
[2]M. Abplanalp, J. Fousek, and P. Günter, Phys. Rev. Lett. **86**, 5799 (2001).
[3]T. Morita and Y. Cho, Appl. Phys. Lett. **84**, 257 (2004).
[4]S. Bühlmann, E. Colla, and P. Muralt, Phys. Rev. B **72**, 214120 (2005).
[5]A. L. Kholkin, I. K. Bdikin, V. V. Shvartsman, and N. A. Pertsev, Nanotechnology **18**, 095502 (2007).
[6]Y. Kim, S. Bühlmann, S. Hong, S. Kim, and K. No, Appl. Phys. Lett. **90**, 072910 (2007).
[7]Y. Kan, H. Bo, X. Lu, W. Cai, Y. Liu, and J. Zhu, Appl. Phys. Lett. **92**, 172910 (2008).
[8]X. Wang, Z. Xu, Z. R. Li, F. Li, H. B. Chen, and S. J. Fan, Ferroelectrics **401**, 173 (2010).
[9]S. Jesse, H. N. Lee, and S. V. Kalinin, Rev. Sci. Instrum. **77**, 073702 (2006).
[10]V. V. Shvartsman, A. L. Kholkin, A. Orlova, D. Kiselev, A. A. Bogomolov, and A. Sternberg, Appl. Phys. Lett. **86**, 202907 (2005).
[11]V. V. Shvartsman and A. L. Kholkin, Phys. Rev. B **69**, 014102 (2004).
[12]B. J. Rodriguez, R. J. Nemanich, A. Kingon, A. Gruverman, S. V. Kalinin, K. Terabe, X. Y. Liu, and K. Kitamura, Appl. Phys. Lett. **86**, 012906 (2005).
[13]W. Ma and D. Hesse, Appl. Phys. Lett. **84**, 2871 (2004).
[14]D. Damjanovic, Rep. Prog. Phys. **61**, 1267 (1998).
[15]A. K. Tagantsev, P. Muralt, and J. Fousek, Mater. Res. Soc. Symp. Proc. **784**, 517 (2004).
[16]I. K. Bdikin, A. L. Kholkin, A. N. Morozovska, S. V. Svechnikov, S. H. Kim, and S. V. Kalinin, Appl. Phys. Lett. **92**, 182909 (2008).
[17]X. F. Du and I. W. Chen, J. Appl. Phys. **83**, 7789 (1998).
[18]S. V. Kalinin and D. A. Bonnell, Nano Lett. **4**, 555 (2004).
[19]J. F. Scott, K. Watanabe, A. J. Hartmann, and R. N. Lamb, Ferroelectrics **225**, 83 (1999).
[20]See supplementary material at http://dx.doi.org/10.1063/1.3562034 for ESR analysis of the PIMNT single crystals.